Electronic Materials Letters (2020) 16:264–275
https://doi.org/10.1007/s13391-020-00211-6

ORIGINAL ARTICLE - NANOMATERIALS

Beneficial Effect of Manganese(II) Ions on the Morphology of Polyol Synthesised Silver Nanowires

C. Prabukumar[1] · **K. Udaya Bhat**[1]

Received: 19 November 2019 / Accepted: 1 March 2020 / Published online: 2 April 2020

Abstract

Silver nanowires (Ag NWs) is a potential material to be used as the transparent conductive electrode (TCE) material, in the flexible electronic applications. The polyol method is the commonly used technique to synthesis the silver nanowires. The growth of the silver nanowires is facilitated by the oxidative etching of the silver seed particles. The present work investigates the influence of the manganese(II) ions to promote the growth of silver nanowires. The manganese(II) ions, due to its multiple oxidation states, play an essential role in removing the dissolved atomic oxygen, which prevent the growth of longer nanowires. Its effect on the length and diameter of the silver nanowires is studied in detail with different concentration levels. Characterization tools, such as X-ray diffractometry, electron microscopy (FESEM and TEM) and UV–VIS spectroscopy are used to characterise the synthesised silver nanowires. The addition of manganese(II) ions alters the aspect ratio of the silver nanowires that in turn, affects the optoelectrical properties of the TCE films. By using the synthesised silver nanowires, transparent heaters are successfully fabricated and their performances under different conditions are evaluated.

Graphic Abstract

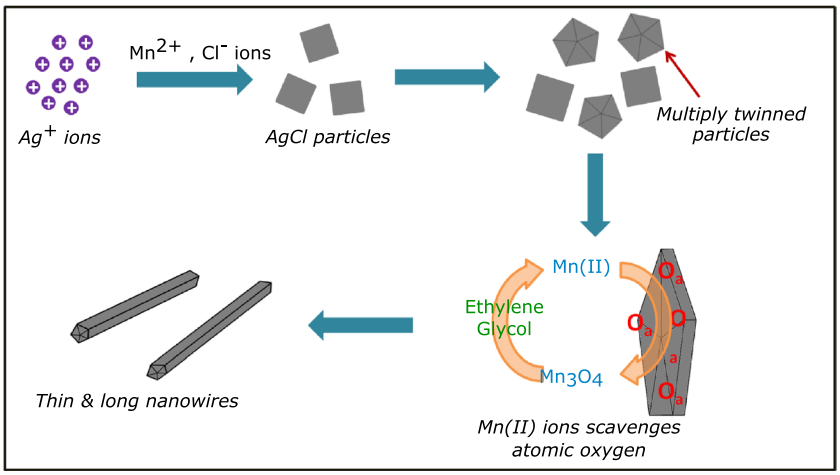

Keywords Silver nanowires · Electronic materials · Oxygen scavenger · Transparent heaters

✉ K. Udaya Bhat
udayabhatk@gmail.com

[1] Department of Metallurgical and Materials Engineering, National Institute of Technology Karnataka, Surathkal, Mangaluru 575025, India

1 Introduction

Recent advances in the field of internet of things (IoT) are set to improve the human health and life with the help of flexible and stretchable devices, such as flexible solar cells [1], foldable displays [2], health monitoring sensor skins [3], transparent heaters [4] and so on [5]. These devices are designed to perform under various mechanical motions. In all these devices, a transparent conductive electrode (TCE) is an essential and critical element. The current TCE market is lead by Indium Tin Oxide (ITO) film coated on PET sheet, mainly due to its high optical transparency (> 90%) and low sheet resistance (< 10 Ω/sq) [6]. But the brittle ITO is often prone to fail when it is subjected to stretching and twisting movements [7]. This raises a concern over the dependability and durability of the devices made using ITO. Alternatively, TCEs are fabricated from carbon nanotubes (CNT) [8], conducting polymers [9], metal nanowires [10, 11] and graphene [12]. The metal nanowires are showing promising results amongst other alternatives in terms of cost, synthesis and fabrication process. The silver nanowires based films have been produced with the optical transparency > 90% and sheet resistance < 10 Ω/sq. [13]. Techniques, such as Meyer-rod coating [14], spray deposition [15], spin coating [16] and printing [17] are employed to fabricate the transparent conductive silver nanowires films. The polyol method is the widely used method to synthesis the silver nanowires [18–20]. The aspect ratio (length to diameter ratio) of silver nanowires used must be high to obtain a highly transparent and conductive film [21]. The one-dimensional growth of the silver nanowires is often hindered by oxidative etching of the silver seed particles during the polyol synthesis process [22]. Wiley et al. [23] and Korte et al. [24] reported that the introduction of Fe(II)/Fe(III) and Cu(I)/Cu(II) ions during the synthesis process prevent the oxidative etching of silver seed particles. This proved to increase the length of the silver nanowires [25] where copper ions showed better results than the iron ions [26]. But the silver nanowires synthesised in the presence of Cu(II) tend to have diameters in the range of 125-250 nm [25]. Many efforts are taken to improve the aspect ratio of the silver nanowires such as multistep synthesis [27], replacing the small chain length PVP molecules with the longer chain length PVP molecules [28], addition of Br^- ions [29], high pressure [30] and N_2 gas atmosphere synthesising [31] along with the use of oxygen scavengers, like copper or iron ions. Despite the improvements achieved by tailoring the other parameters, the presence of oxygen scavengers (like Cu/Fe ions) remains crucial in the synthesis of silver nanowires.

The present work is solely focussed on the prospect of improving the aspect ratio of silver nanowires with the use of alternative oxygen scavenger. The manganese (Mn) ions are explored as the oxygen scavenger in place of Cu or Fe ions in the polyol synthesis of silver nanowires. The characteristics of manganese, such as (1) tendency to absorb more oxygen owing to its high negative free energy for oxidation; (2) large number of oxidation states (2, +3, +4, +5, +6 and +7) compared to that of Cu (+1 and +2) and Fe (+2 and +3) is expected to help in removing the oxygen effectively from the surface of silver seed particles. So the silver nanowires synthesised with the addition of Mn(II) ions may have a smaller diameter and higher aspect ratio than that synthesised with the addition of Fe or Cu ions. These are the important factors of the silver nanowires required to fabricate the high transparent and conductive films.

In this work, the conventional polyol method is adopted but with the rapid addition of silver precursor. In conventional polyol method, the silver precursor addition is done slowly [25, 32, 33].

2 Experimental Details

2.1 Synthesis of Silver Nanowires

To synthesis silver nanowires (Ag NWs) by polyol method, solutions of silver nitrate ($AgNO_3$), polyvinylpyrrolidone (PVP, M.W. = 40,000), NaCl (44.5 mM), $CuCl_2{\cdot}5H_2O$ (22 mM) and $MnCl_2{\cdot}4H_2O$ (22 mM, 40 mM and 65 mM) were prepared by using ethylene glycol (EG) as solvent. A flask containing 15 ml solution of 0.147 M PVP was heated for 45 min at 170 °C in an oil bath under magnetic stirring. Then, 75 µL of chloride solution ($NaCl/CuCl_2{\cdot}5H_2O/MnCl_2{\cdot}4H_2O$) was added into the flask. After 3 min, 3 ml $AgNO_3$ (0.153 M) solution was added into the flask at once. Upon adding $AgNO_3$, the solution was continued to be heated for another 2 h. Then the solution was removed from the oil bath and allowed to cool. Finally, the as-synthesised product was washed with acetone and isopropyl alcohol by following solvent-aid precipitation decantation method [34]. The washed silver nanowires dispersion was diluted with the IPA and stored in a vial. The silver nanowires films were prepared by spray coating technique. The silver nanowires dispersed in IPA was loaded into a commercial airbrush kit and spray-coated on the glass substrate kept on a hot plate at 80 °C. The air pressure used was 68.9 kPa (10 psi). The distance between the spray gun and the substrate was 15 cm. Later, the prepared silver nanowires films were subjected to annealing at 165 °C for 30 min.

2.2 Characterization

The structural property was characterized by using X-ray diffractometer (JDX 8P, JEOL), with monochromatic Cu K_α ($\lambda = 0.154$ nm) radiation. The morphological studies were carried out by using field emission scanning electron microscope (Carl Zeiss, Sigma). TEM studies were performed by using transmission electron microscope (JEM-2100, JEOL). UV–VIS absorption spectra were obtained by using UV–VIS spectrometer (SD2000, Ocean Optics). The sheet resistance of the silver nanowires films was measured by using four-probe measurement setup (SES instruments, India).

2.3 Testing of Silver Nanowires Film

To test the mechanical flexibility, the silver nanowires film was spray-coated on a flexible plastic film. The prepared film was bent to 4.5 mm radius of curvature for 500 bending cycles. The heater test was performed by applying the electrical potential between two ends of the silver nanowires film using Keithley 2400 source meter. The temperature generated on the film was measured by using infrared thermometer (HT-826; Temp. resolution = 0.1° C).

3 Results and Discussion

3.1 Ag NWs Synthesised with Different Chloride Condition

The FESEM micrographs in Fig. 1 show the morphology of the silver products synthesised by using the polyol method with four different types of chloride solutions. The concentration of each chloride salts was chosen to have almost equal amount of Cl^- ions in the reaction solution. The product synthesised without the addition of any chloride lead to the growth of silver particles with an average size of 330 nm, with the size range 110 nm to 1 µm. When the solution of $AgNO_3$ was introduced into the reaction solution, the silver ions (Ag^+ ions) reduced to Ag^0 rapidly. Instead of growing into one-dimensional nanowires, the reduced silver nanoparticles aggregated to grow into coarser silver particles by Ostwald ripening process [33].

However, the micrograph shown in Fig. 1b reveals that the addition of NaCl promoted the growth of one-dimensional nanorods along with the cubes (avg. size = 74 nm) and pyramid (avg. size = 119 nm) particles. The rapid reduction of Ag^+ ions to Ag^0 was avoided by the formation of AgCl. This AgCl acted as the buffer phase to ensure the controlled release of silver into the reaction for the one-dimensional growth [33]. Hence, the presence of Cl^- ions during the

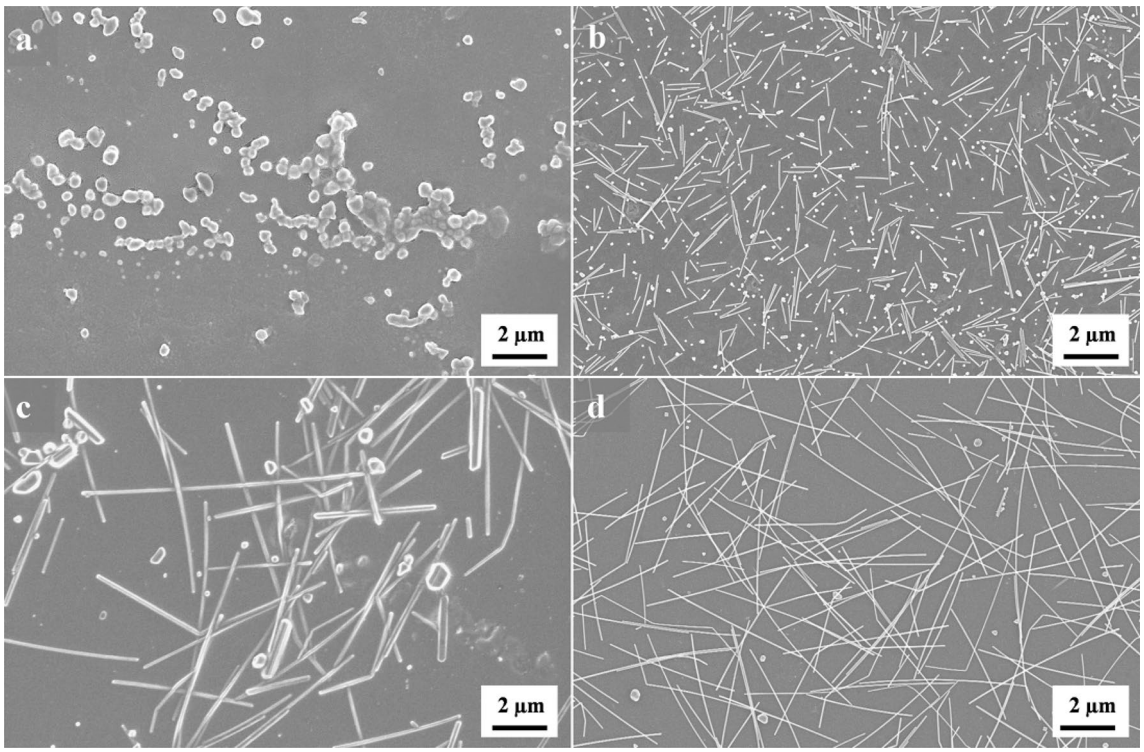

Fig. 1 FESEM micrographs of the silver products synthesised with the addition of **a** no chloride; **b** NaCl; **c** $CuCl_2{\cdot}5H_2O$ and **d** $MnCl_2{\cdot}4H_2O$

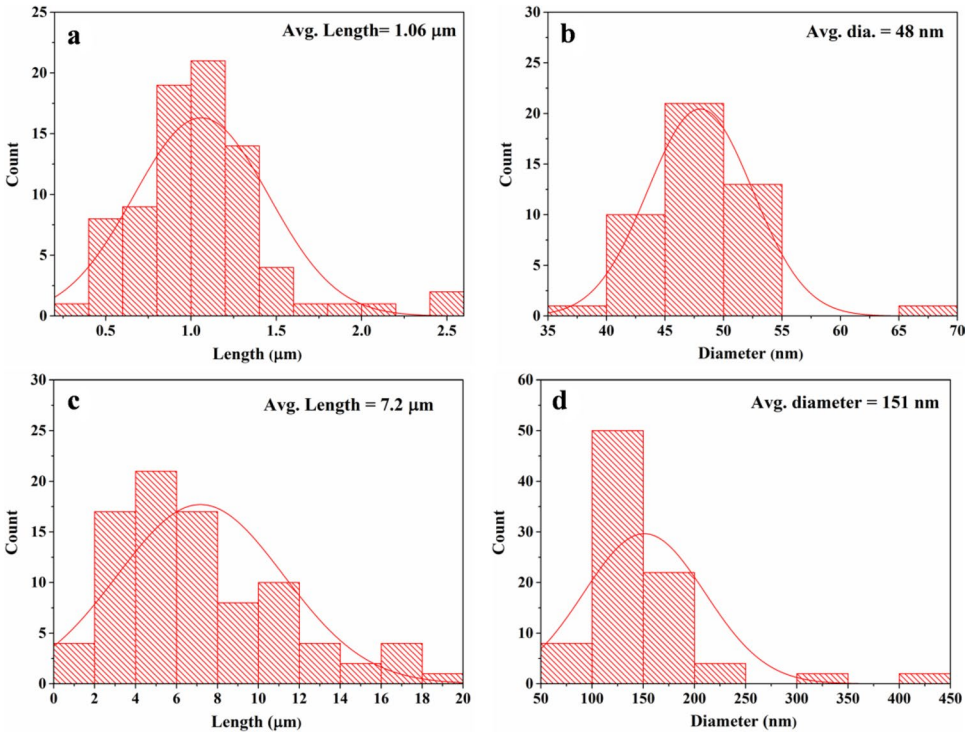

Fig. 2 Length and diameter distribution: **a**, **b** silver nanorods synthesised with the addition of NaCl; **c**, **d** silver nanowires synthesised with the addition of $CuCl_2$

synthesis process is important to prevent the formation of large silver particles and to promote one-dimensional growth of the silver. The mean length of the silver nanorods is 1 µm (Fig. 2a). It is very small to be used for the TCE application. The growth of the short nanorods was the result of oxygen etching of the silver twinned particles. During the synthesis, the atomic oxygen (O_a) present in the reaction solution tends to etch away the twinned particles that otherwise serve as seeds for the silver nanowires growth. The etching of twinned seed particles leads to the growth of shorter nanowires or nanorods [22].

The addition of copper chloride in place of NaCl is a proven approach to act against the problem of oxygen etching of twinned particles. The length of the silver nanowires (Fig. 1c) was enhanced up to 7.2 µm with the maximum length up to 20 µm (Fig. 2c) when NaCl is replaced with the copper chloride. The introduction of copper ions into the reaction through copper chloride prevented the etching of the twins by scavenging the atomic oxygen from the surface of the twinned silver particles [24]. But, there is a concern with the diameter of the nanowires. The average diameter the nanowires synthesised with the addition of copper ions was measured as 151 nm (Fig. 2d). Although the added copper ions helped to enhance the length of the silver nanowires, it also increases the diameter of the nanowires. The formation of large diameter (125 to 250 nm) nanowires with the presence of copper ions is already reported [25].

The large diameter silver nanowires would block more light when it is used to fabricate TCE film. As a result, the optical transparency of the film is expected to reduce. Many efforts were taken in recent times to decrease the diameter of the silver nanowires by optimizing the other parameters, like the use of longer chain length PVP molecules [28, 35] or use of Br^- ions [29], introducing benzoin-derived radicals [31], high pressure [30, 36] and N_2 gas environment synthesis [31]. As mentioned earlier, the present work explored the use of manganese ions as an alternate oxygen scavenger to iron and copper ions without changing any other synthesis parameters.

3.2 Ag NWs Synthesised with $MnCl_2$

FESEM micrographs of the silver nanowires synthesised with different concentrations of $MnCl_2$, their length and diameter distribution are shown in Fig. 3. The maximum and average length of the nanowires synthesised with 22 mM of $MnCl_2$ was measured as 16 µm and 5.2 µm, respectively. But increase in the concentration to 40 mM increased the length of the nanowires. The maximum and average lengths were measured as 20 µm and 7.7 µm, respectively. When the $MnCl_2$ concentration was further increased to 65 mM the longitudinal and diameter wise direction growth was relatively reduced compared to that of the previous concentration. The measured maximum and average length of the nanowires was 16 µm and 6.3 µm respectively.

Meanwhile, the average diameter of the synthesised silver nanowires was measured as 60 nm, 80 nm and 71 nm for the concentration of 22 mM, 40 mM and 65 mM respectively.

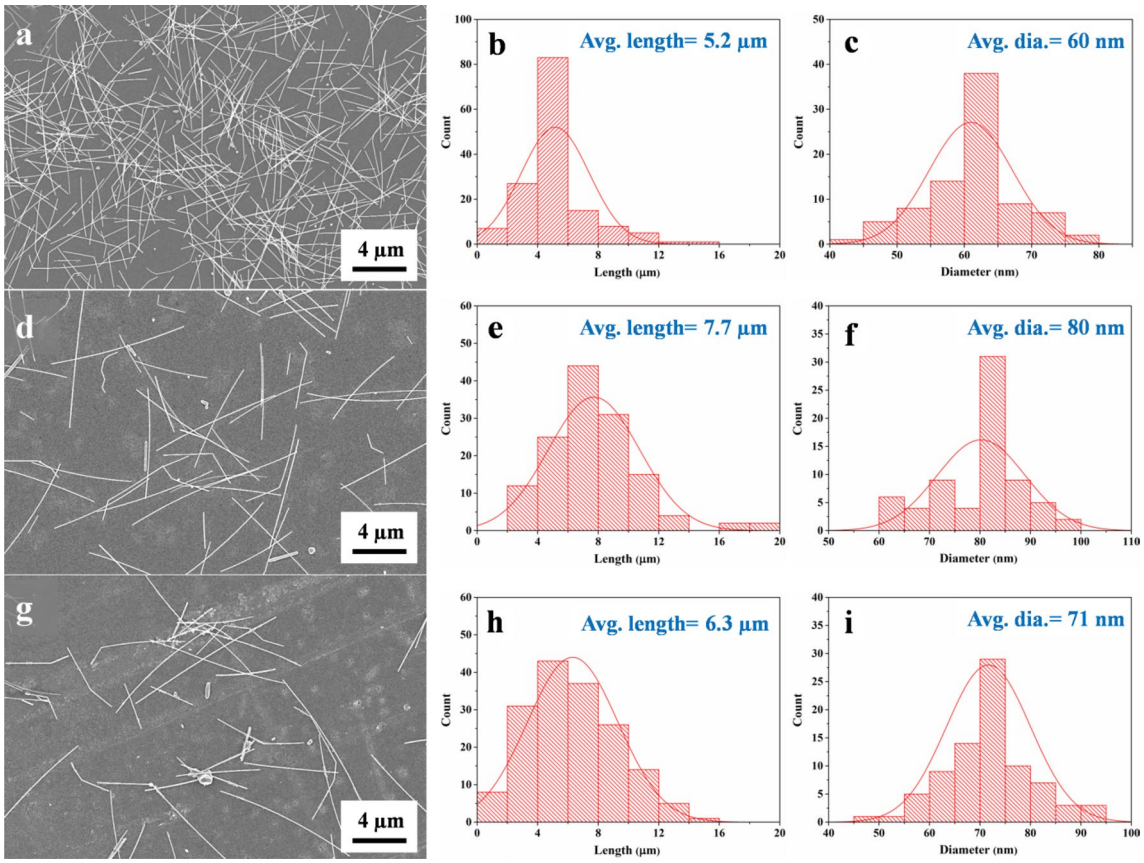

Fig. 3 FESEM micrographs of the silver nanowires synthesised with the addition of $MnCl_2$ of different concentrations **a** 22 mM, **d** 40 mM, **g** 65 mM; their corresponding length (**b**, **e**, **h**) and diameter distribution (**c**, **f**, **i**)

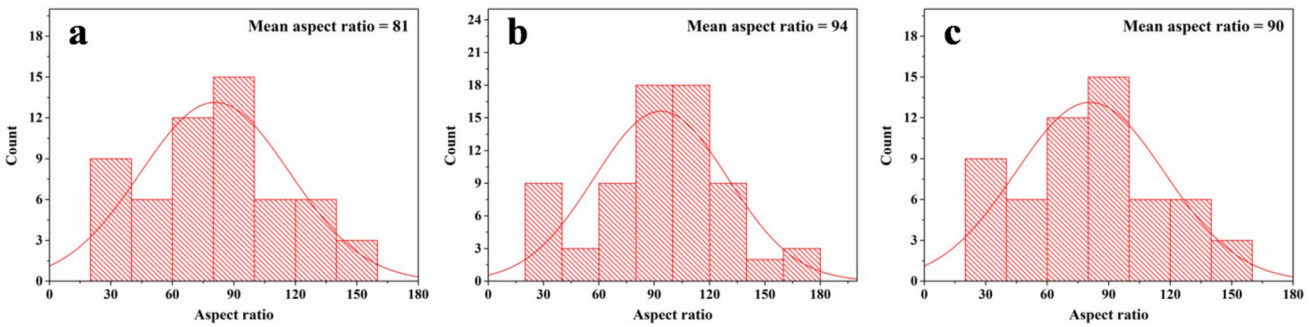

Fig. 4 Aspect ratio distributions of silver nanowires synthesised with the addition of $MnCl_2$ of concentration **a** 22 mM, **b** 40 mM and **c** 65 mM

Though 40 mM sample is reported to have large diameter, its corresponding length is longer compared to that of other samples. The aspect ratio (length to diameter) of the silver nanowires was calculated for silver nanowires synthesised with the addition of three different $MnCl_2$ concentration samples (Fig. 4). The mean aspect ratio of 40 mM concentration sample was the highest among all the silver nanowires samples. The high aspect ratio of silver nanowires will be beneficial to improve the percolation path that in turn will increase the electrical conductivity of the silver nanowires film fabricated by using this sample.

Figure 5a shows the UV–VIS absorption spectra of the silver particles synthesised without any chloride salt, silver nanowires synthesised with the addition of $CuCl_2$ (22 mM) and $MnCl_2$ (22 mM). The absorption spectrum of silver particles showed a broad absorption peak at 450 nm. The silver nanowires exhibited a predominant peak along with a low intensity peak. The $CuCl_2$ sample showed maximum

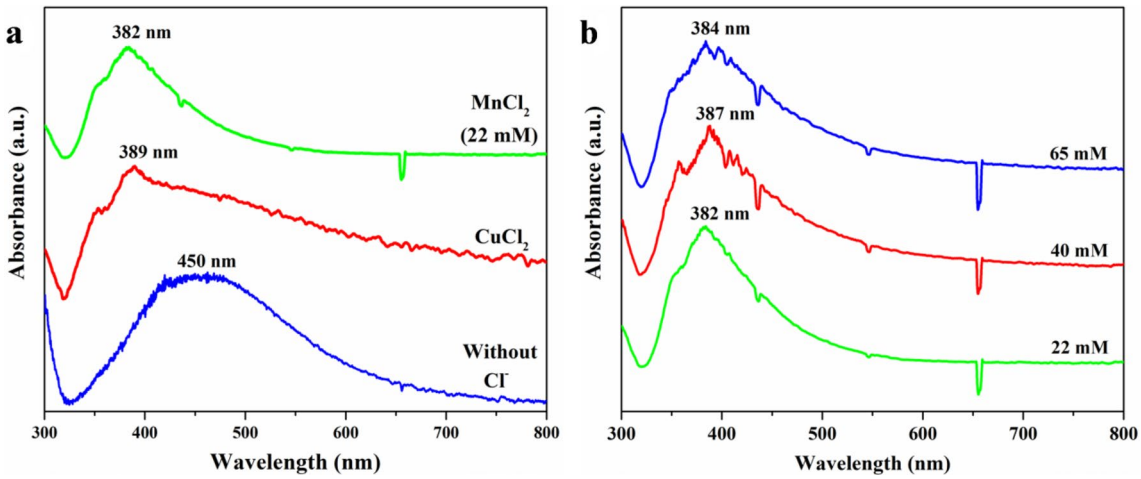

Fig. 5 UV–VIS absorption spectra of **a** silver products synthesised with three different chloride conditions; **b** silver nanowires synthesised with the addition of different concentrations of $MnCl_2$

absorption at 389 nm while $MnCl_2$ sample exhibited the maximum absorption at 382 nm. The existence of these observed peaks was due to the surface plasmon resonance (SPR) of silver nanostructures [26]. The SPR peak at the 450 nm is attributed to the large particle size of silver [37]. However, the maximum absorption shifts to smaller wavelength for the nanowires. This is because the surface plasmon resonance becomes dominant in the transverse direction [26].

The blue-shift from 389 nm to 382 nm is attributed to the decrease in the diameter of the nanowires from 151 to 60 nm [31]. Similarly, the shift in the absorption peak was also observed for the silver nanowires synthesised with different $MnCl_2$ concentration (Fig. 5b). The 22 mM sample with a mean diameter of 60 nm exhibited the absorption peak at 382 nm. But the absorption was red-shifted to 387 nm for 40 mM sample because of its larger diameter of 80 nm. This red-shift of SPR peak with respect to increase in the diameter was attributed to the inhomogeneous polarization caused by the existence of multipolar oscillations in the silver nanowires due to the large diameter [26, 38]. The absorption peak was blue-shifted to 384 nm for the 65 mM sample as the result of decrease in the diameter to 71 nm from 80 nm. The change in the absorption wavelength corresponding to the concentration of the $MnCl_2$ again confirms the influence of Mn(II) ions on the diameter of the silver nanowires [26, 31].

The schematic shown in Fig. 6 explains the influence of Mn(II) ions on the growth of the silver nanowires. During the synthesis, when Ag^+ ions are reduced to Ag^0 to form nuclei, the twins are formed due to the availability of the thermal energy. Multiply-twinned decahedra twins are the most stable and more favorable one to form. These multiply twinned particles (MTP) acts as the seeds for silver

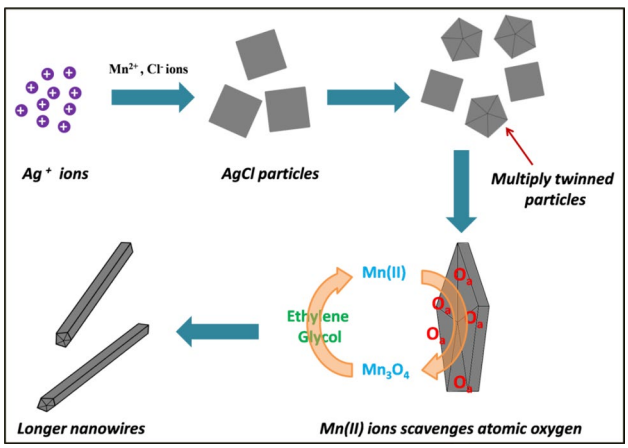

Fig. 6 Schematic shows the role of Mn(II) ions as oxygen scavenger in preventing oxidative etching of the silver seeds

nanowires growth [33]. But this growth is often affected by atomic oxygen, dissociated molecular oxygen from EG, adsorbed on these seed particles. The adsorbed oxygen block the surface of seed particles for the addition of new silver species [24]. This eventually results in the formation of nanocubes or short nanorods instead of nanowires [22]. When Mn(II) ions are introduced into the reaction through $MnCl_2$, the Mn(II) ions get oxidized to higher oxidation state by absorbing the atomic oxygen from the surfaces of the seed particles. The oxidized manganese ions are subsequently reduced back to Mn(II) state by the ethylene glycol [39]. This oxidation and reduction process of Mn ions is continued to remove or scavenge the oxygen which blocks the growth of the nanowires. Thus, the active {111} sites on the twinned seed particles remain available for the addition of new silver species.

When the Mn(II) ions absorb oxygen from the surface of silver seed particles, the following are the possible compounds to be formed, namely, Mn_3O_4, Mn_2O_3 and MnO_2. Among the oxides of Mn, Gibbs free energy of formation (ΔG_f°) for Mn_3O_4 is more negative compared to other manganese oxide compounds. In the case of Cu(I) ions, it will move up to Cu(II) state by absorbing the atomic oxygen. So, the CuO is the expected compound to be formed. The ΔG_f° for Mn_3O_4 is -1288.23 kJ mol^{-1} whereas ΔG_f° for CuO is -129.7 kJ mol^{-1}. Here, the $MnCl_2$ and $CuCl_2$ are the reactants and Mn_3O_4 and CuO are their corresponding products. The ΔG_f° for oxygen scavenging is calculated as,

$$\Delta G_f^\circ \text{ of } \left(MnCl_2 \rightarrow Mn_3O_4\right) = -1288.23 \text{ kJ mol}^{-1} - \left(-440.53 \text{ kJ mol}^{-1}\right) = -847.7 \text{ kJ mol}^{-1}$$

$$\Delta G_f^\circ \text{ of } \left(CuCl_2 \rightarrow CuO\right) = -129.704 \text{ kJ mol}^{-1} - \left(-161.92 \text{ kJ mol}^{-1}\right) = 32.216 \text{ kJ mol}^{-1}$$

The more negative of ΔG_f° of ($MnCl_2 \rightarrow Mn_3O_4$) indicates that the process of oxygen scavenging is more spontaneous than that observed by using Cu(II) ions. In other words, the tendency to absorb oxygen from the surface of silver seed particles is high for Mn(II) ions compared to Cu(I) ions.

The TEM micrograph (Fig. 7a) confirms the aggregation of silver particles when no chloride was used during the synthesis. Figure 7b, c shows the nanorod and nanocube synthesised with the addition of NaCl. The presence of twin boundaries in the nanorod is seen parallel to its axis. The nanocube does not show any evidence for the presence of the twins. It's corresponding SAED pattern (Fig. 7d) confirms the same. From the above observation, it is concluded that the oxidative etching was the reason for the growth of the short nanorods and nanocubes.

XRD pattern (Fig. 8a) of the synthesised silver nanowires show peaks at 38.1°, 44.2° and 64.4° which are corresponding to (111), (200) and (220) planes of silver (JCPDS 04-0783), respectively. The higher peak intensity of (111) plane is attributed to the preferred (111) plane growth of the silver nanowires. Figure 8b shows the TEM micrograph of the silver nanowires synthesised with the addition

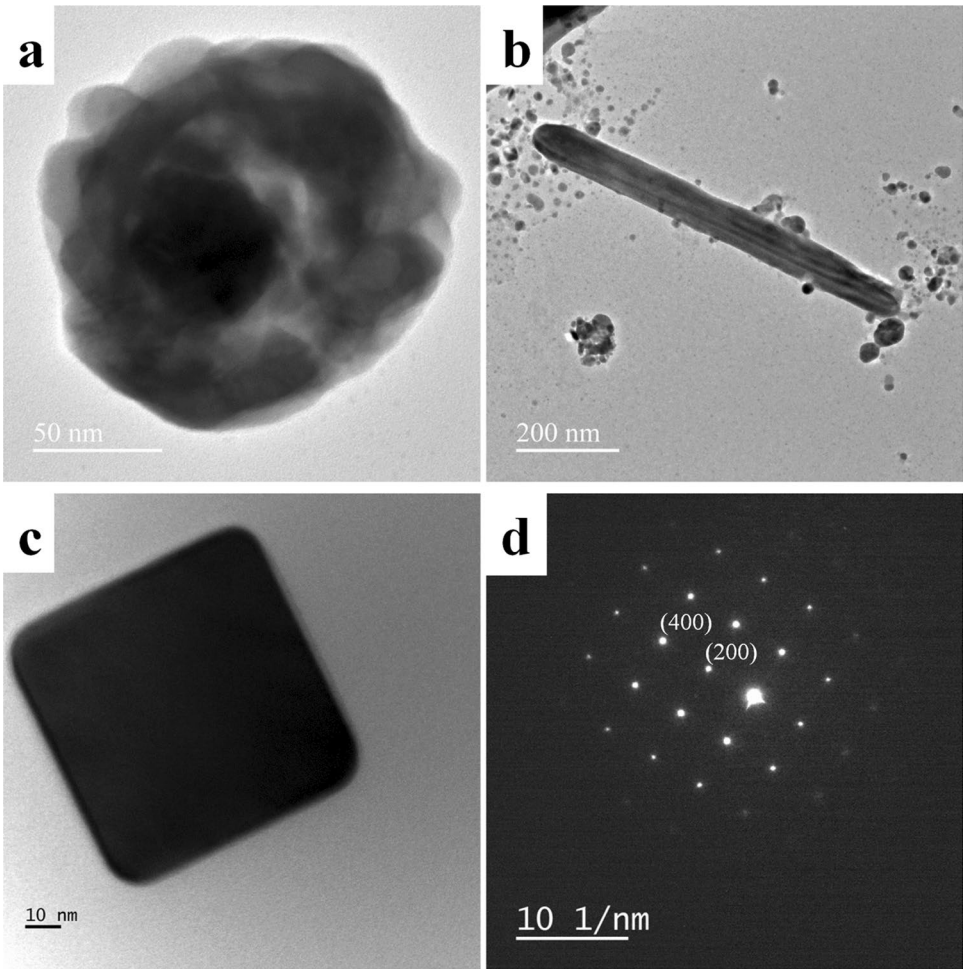

Fig. 7 TEM micrographs of **a** the Ag nanoparticles synthesised with the addition of no chloride salt; **b** Ag nanorod and **c** Ag nanocube synthesised with the addition of NaCl and **d** the corresponding SAED pattern of Ag nanocube

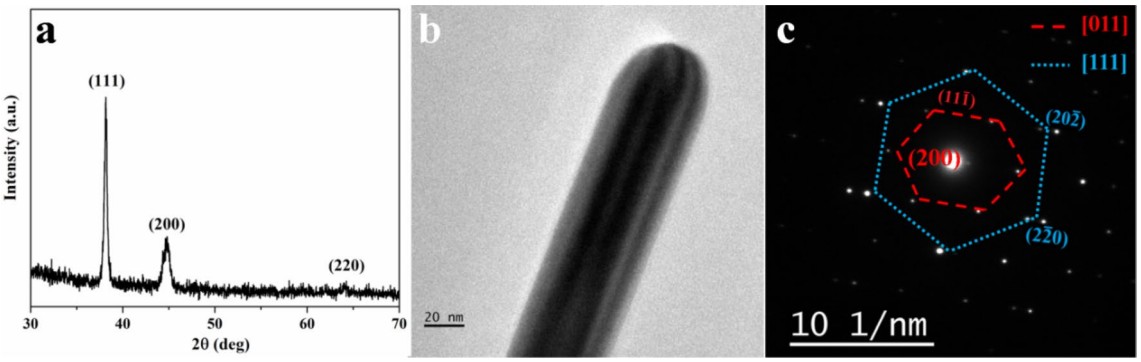

Fig. 8 **a** XRD pattern; **b** TEM micrograph and **c** SAED pattern of the silver nanowires synthesised with 22 mM of $MnCl_2$

of $MnCl_2$ (22 mM). The presence of the twin boundaries along the longitudinal axis of the nanowire is seen in the micrograph (Fig. 8b). It is observed that the diameter of the nanowires was 50 nm. The selected area electron diffraction (SAED) pattern shown in Fig. 8c confirmed the presence of twins in the silver nanowire. Two different sets of diffraction patterns with the zone axis of [011] and [111] were observed. The existence of two sets of diffraction in the SAED pattern is supported by the previous report [40].

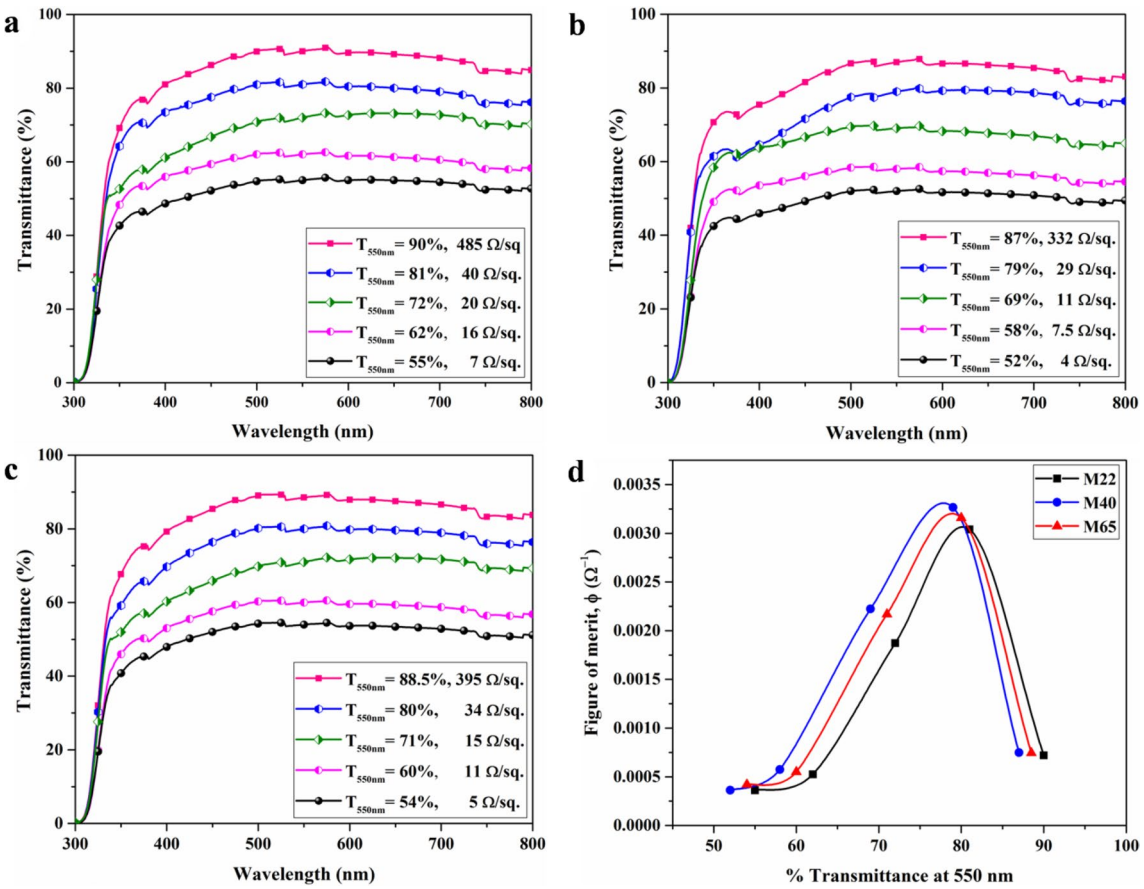

Fig. 9 Optical transmittance and sheet resistance of the silver nanowires films prepared by using **a** 22 mM; **b** 40 mM; **c** 65 mM concentration of $MnCl_2$ sample; **d** figure of merits of films prepared by using 22 mM, 40 mM, 65 mM concentration of $MnCl_2$ samples

3.3 Characterization and Testing of Ag NWs Films

Figure 9a–c show the UV–VIS transmittance spectra of the films prepared by using silver nanowires synthesised with the three different concentrations of $MnCl_2$ (22 mM, 40 mM and 65 mM). The films prepared by using 22 mM, 40 mM and 65 mM samples are named as M22, M40 and M65 respectively. The spray coating method was followed to prepare the multilayer (4L, 5L, 6L, 7L and 8L) silver nanowires films. The density of the silver nanowires film was increased with respect to the number of spray-coated layers. Figure 9a shows the transmittance spectra of M22 films with their corresponding sheet resistance (R_s) values. The transmittance at $\lambda = 550$ nm ($\%T_{550\ nm}$) and R_s values of 4L, 5L, 6L, 7L and 8L are 90%, 81%, 72%, 62%, 55% and 485, 40, 20, 16 and 7 Ω/sq, respectively. With high R_s (4L film) of 485 Ω/sq and low $\%T_{550\ nm}$ of less than 75%, the films other than 5L are not suitable to be used as TCE. The 5L film is the best TCE among M22 films with the optical transmittance of 81% and sheet resistance of 40 Ω/sq. Similarly, among M40 and M65 films, the 5L film of each set showed the acceptable transmittance and sheet resistance with the values $\%T_{550\ nm} = 79\%$, $R_s = 29$ Ω/sq and $\%T_{550\ nm} = 80\%$, $R_s = 34$ Ω/sq, respectively. The figure of merit is the widely accepted quantitative expression that defines the quality of a transparent conductive electrode film. The figure of merits or FOM (φ_{TC}) is calculated by using the formula given by Haacke [41],

$$\varphi_{TC} = T^{10}/R_s \quad (1)$$

The term 'T' and 'R_s' are the optical transmittance and the sheet resistance of the film, respectively. The FOM values of 5L films from each set of films were calculated by using the formula (1). The calculated values are showed with their sheet resistance in Fig. 9d. The maximum value of 0.00327 Ω^{-1} was reported for the 5L-M40 film. The FOM value of 5L-M65 and 5L-M22 were reported as 0.00316 Ω^{-1} and 0.00304 Ω^{-1}, respectively. The figure of merit is also represented as the ratio of electrical to optical conductivity (σ_{DC}/σ_{OP}). The σ_{DC}/σ_{OP} ratio is calculated using the formula [42],

$$T = (1 + [188.5/R_s) \cdot (\sigma_{OP}/\sigma_{DC})]^{-2} \quad (2)$$

The calculated σ_{DC}/σ_{OP} ratio for 5L-M22, 5L-M40 and 5L-M65 are 42.4 Ω^{-1}, 52 Ω^{-1} and 46.97 Ω^{-1}, respectively. The maximum FOM values calculated from the above two formula belonged to 5L-M40 film. Although large diameter factor of the silver nanowires (40 mM sample) caused to reduce the optical transmittance of M40 sample to 79%, the low sheet resistance of 29 Ω/sq was obtained because of increased length of the nanowires. The use of longer silver nanowires improved the percolation path while reducing the wire to wire contact resistance in the film. That eventually lead to high FOM value.

The silver nanowires coated on the plastic film and commercial ITO/PET film (Sigma-Aldrich) were subjected to the bending test. The percentage change in the sheet resistance of both films with respect to the bending cycles is shown in Fig. 10a. The sheet resistance of the ITO film increased up to 275% from its original value after the 280 bending cycles. On the other hand, the prepared silver nanowires film showed better mechanical flexibility with only 14% increase from its original sheet resistance after 500 cycles of bending. The camera image of the silver nanowires film is shown in Fig. 10b.

The 5L silver nanowires film of sets M22, M40 and M65 having the sheet resistance of 40, 29 and 34 Ω/sq, respectively were tested for the heater application. The heater test was conducted at the applied voltage of 5, 7 and 10 V. The temperature of the silver nanowires film in response to the applied voltage was recorded at the time interval of 15 s. The temperature versus time profiles of silver nanowires films

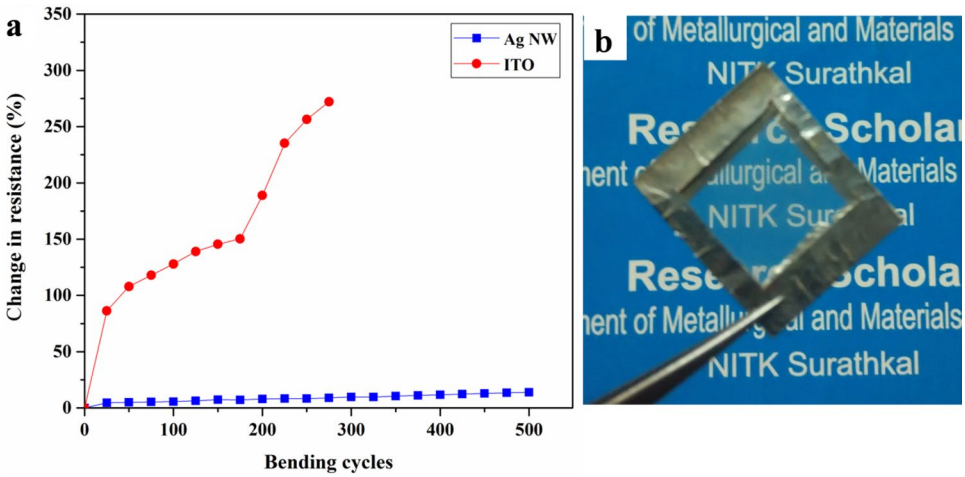

Fig. 10 **a** Change in sheet resistance value of the silver nanowires film and ITO film against the number of bending cycles; **b** camera image of the silver nanowires film

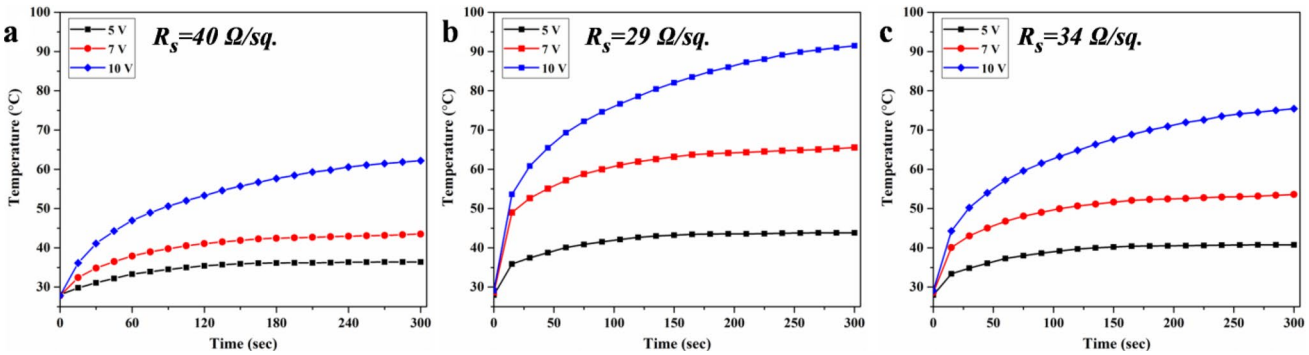

Fig. 11 Temperature versus time curve (heater test) of the silver nanowires films (M22, M40, M65, respectively) at applied voltage values of 5, 7 and 10 V

corresponding to applied voltages are shown in Fig. 11. From the temperature versus time curve shown in Fig. 11a, it is observed that the temperature of the silver nanowires film increased with respect to time of the voltage supply. The silver nanowires film of $R_s = 40$ Ω/sq attained the maximum temperature of 62 °C in 300 s at the applied voltage of 10 V. While the silver nanowires film of 34 Ω/sq reached higher temperature of 74 °C for the same voltage. But the highest temperature of 90 °C was attained by the silver nanowires film of $R_s = 29$ Ω/sq at the voltage of 10 V. The same film reached the temperature of 65 °C when the applied voltage is 7 V. When the sheet resistance of the nanowires film is low the performance of the heater is high [43].

The present study explored the effect of Mn(II) ions during the synthesis of silver nanowires. The results showed that the length and diameter of the nanowires could be manipulated by introducing Mn(II) ions during the growth. It shows the potential of Mn(II) to play a role in synthesising process of the silver nanowires to produce better transparent conductive electrodes.

4 Conclusions

The role of manganese(II) ions as the oxygen scavenger during the synthesis of silver nanowires was explored. The addition of $MnCl_2$ promoted the one-directional growth of silver nanowires. The silver nanowires synthesised with the presence of Mn(II) ions was reported to have a diameter of 60 nm compared to 151 nm when widely used Cu(II) ions was added. Among three different concentrations of $MnCl_2$, the 40 mM concentration sample showed longest nanowires with highest aspect ratio. The reason is due to the effectiveness of Mn(II) ions in removing atomic oxygen from the surface of silver seed particles. It is supported thermodynamically with the help of Gibbs free energy of formation. The oxygen scavenging process was more spontaneous when Mn(II) ions were used. The Ag NWs films prepared using 40 mM sample showed good optoelectrical characteristics with the $T_{550nm} = 79\%$ and $R_s = 29$ Ω/sq. The transparent heater test conducted showed that the Ag NWs film generated high temperature of 90 °C at the applied volt of 10 V. The flexible Ag NWs film deposited on a plastic substrate exhibited good mechanical flexibility with small change in sheet resistance of 14% after 500 bending cycles. Hence, we conclude that the addition of Mn(II) ions in the synthesis process will positively affect the silver nanowires formation.

Acknowledgements Prabukumar would like to thank NIT Karnataka for providing financial support in the form of Institute fellowship. The author is thankful to Dr. Saumen Mandal, Assistant Professor, Department of Metallurgical and Materials Engineering, NITK for providing four-probe measurement setup and Prof. M. N. Satyanarayan, Department of Physics, NITK for providing UV–VIS spectroscopy and Keithley 2400 source meter. The author wants to thank Mr. Prashant Huilgol and Mr. M. S. Nandana, Department of Metallurgical and Materials Engineering, NITK for their help in TEM images.

References

1. Kim, B.J., Kim, D.H., Lee, Y.Y., Shin, H.W., Han, G.S., Hong, J.S., Mahmood, K., Ahn, T.K., Joo, Y.C., Hong, K.S., Park, N.G., Lee, S., Jung, H.S.: Highly efficient and bending durable perovskite solar cells: toward a wearable power source. Energy Environ. Sci. **8**, 916–921 (2015)
2. Ok, K.H., Kim, J., Park, S.R., Kim, Y., Lee, C.J., Hong, S.J., Kwak, M.G., Kim, N., Han, C.J., Kim, J.W.: Ultra-thin and smooth transparent electrode for flexible and leakage-free organic light-emitting diodes. Sci. Rep. **5**, 9464 (2015)
3. Trung, T.Q., Ramasundaram, S., Hwang, B.U., Lee, N.E.: An all-elastomeric transparent and stretchable temperature sensor for body-attachable wearable electronics. Adv. Mater. **28**, 502–509 (2016)
4. Jang, J., Hyun, B.G., Ji, S., Cho, E., An, B.W., Cheong, W.H., Park, J.-U.: Rapid production of large-area, transparent and stretchable electrodes using metal nanofibers as wirelessly operated wearable heaters. NPG Asia Mater. **9**, e432 (2017)

5. Zhan, Y., Mei, Y., Zheng, L.: Materials capability and device performance in flexible electronics for the Internet of Things. J. Mater. Chem. C **2**, 1220–1232 (2014)
6. Sibin, K.P., Srinivas, G., Shashikala, H.D., Dey, A., Sridhara, N., Sharma, A.K., Barshilia, H.C.: Highly transparent and conducting ITO/Ag/ITO multilayer thin films on FEP substrates for flexible electronics applications. Sol. Energy Mater. Sol. Cells **172**, 277–284 (2017)
7. Chen, Z., Cotterell, B., Wang, W., Guenther, E., Chua, S.J.: A mechanical assessment of flexible optoelectronic devices. Thin Solid Films **394**, 201–205 (2001)
8. Mirri, F., Ma, A.W., Hsu, T.T., Behabtu, N., Eichmann, S.L., Young, C.C., Tsentalovich, D.E., Pasquali, M.: High-performance carbon nanotube transparent conductive films by scalable dip coating. ACS Nano **6**, 9737–9744 (2012)
9. Zhang, Y., Wu, Z., Li, P., Ono, L.K., Qi, Y., Zhou, J., Shen, H., Surya, C., Zheng, Z.: Fully solution-processed TCO-free semitransparent perovskite solar cells for tandem and flexible applications. Adv. Energy Mater. **8**, 1701569 (2018)
10. Guo, H., Lin, N., Chen, Y., Wang, Z., Xie, Q., Zheng, T., Gao, N., Li, S., Kang, J., Cai, D., Peng, D.L.: Copper nanowires as fully transparent conductive electrodes. Sci. Rep. **3**, 2323 (2013)
11. Chang, M.H., Cho, H.A., Kim, Y.S., Lee, E.J., Kim, J.Y.: Thin and long silver nanowires self-assembled in ionic liquids as a soft template: electrical and optical properties. Nanoscale Res. Lett. **9**, 330 (2014)
12. De Castro, R.K., Araujo, J.R., Valaski, R., Costa, L.O.O., Archanjo, B.S., Fragneaud, B., Cremona, M., Achete, C.A.: New transfer method of CVD-grown graphene using a flexible, transparent and conductive polyaniline-rubber thin film for organic electronic applications. Chem. Eng. J. **273**, 509–518 (2015)
13. Xu, F., Xu, W., Mao, B., Shen, W., Yu, Y., Tan, R., Song, W.: Preparation and cold welding of silver nanowire based transparent electrodes with optical transmittances > 90% and sheet resistances < 10 ohm/sq. J. Colloid Interface Sci. **512**, 208–218 (2018)
14. Zhu, S., Gao, Y., Hu, B., Li, J., Su, J., Fan, Z., Zhou, J.: Transferable self-welding silver nanowire network as high performance transparent flexible electrode. Nanotechnology **24**, 335202 (2013)
15. Ding, Z., Stoichkov, V., Horie, M., Brousseau, E., Kettle, J.: Spray coated silver nanowires as transparent electrodes in OPVs for Building Integrated Photovoltaics applications. Sol. Energy Mater. Sol. Cells **157**, 305–311 (2016)
16. Tang, Q., Shen, H., Yao, H., Jiang, Y., Zheng, C., Gao, K.: Preparation of silver nanowire/AZO composite film as a transparent conductive material. Ceram. Int. **43**, 1106–1113 (2017)
17. He, X., He, R., Lan, Q., Wu, W., Duan, F., Xiao, J., Zhang, M., Zeng, Q., Wu, J., Liu, J.: Screen-printed fabrication of PEDOT: PSS/silver nanowire composite films for transparent heaters. Materials **10**, 220 (2017)
18. Sun, Y., Yin, Y., Mayers, B.T., Herricks, T., Xia, Y.: Uniform silver nanowires synthesis by reducing $AgNO_3$ with ethylene glycol in the presence of seeds and poly (vinyl pyrrolidone). Chem. Mater. **14**, 4736–4745 (2002)
19. Lin, J.Y., Hsueh, Y.L., Huang, J.J., Wu, J.R.: Effect of silver nitrate concentration of silver nanowires synthesized using a polyol method and their application as transparent conductive films. Thin Solid Films **584**, 243–247 (2015)
20. Amirjani, A., Fatmehsari, D.H., Marashi, P.: Interactive effect of agitation rate and oxidative etching on growth mechanisms of silver nanowires during polyol process. J. Exp. Nanosci. **10**, 1387–1400 (2015)
21. De, S., King, P.J., Lyons, P.E., Khan, U., Coleman, J.N.: Size effects and the problem with percolation in nanostructured transparent conductors. ACS Nano **4**, 7064–7072 (2010)
22. Wiley, B., Herricks, T., Sun, Y., Xia, Y.: Polyol synthesis of silver nanoparticles: use of chloride and oxygen to promote the formation of single-crystal, truncated cubes and tetrahedrons. Nano Lett. **4**, 1733–1739 (2004)
23. Wiley, B., Sun, Y., Xia, Y.: Polyol synthesis of silver nanostructures: control of product morphology with Fe(II) or Fe(III) species. Langmuir **21**, 8077–8080 (2005)
24. Korte, K.E., Skrabalak, S.E., Xia, Y.: Rapid synthesis of silver nanowires through a CuCl-or $CuCl_2$-mediated polyol process. J. Mater. Chem. **18**, 437–441 (2008)
25. Bob, B., Machness, A., Song, T.B., Zhou, H., Chung, C.H., Yang, Y.: Silver nanowires with semiconducting ligands for low-temperature transparent conductors. Nano Res. **9**, 392–400 (2016)
26. Ma, J., Zhan, M.: Rapid production of silver nanowires based on high concentration of $AgNO_3$ precursor and use of $FeCl_3$ as reaction promoter. RSC Adv. **4**, 21060–21071 (2014)
27. Li, B., Ye, S., Stewart, I.E., Alvarez, S., Wiley, B.J.: Synthesis and purification of silver nanowires to make conducting films with a transmittance of 99%. Nano Lett. **15**, 6722–6726 (2015)
28. Sonntag, L., Eichler, F., Weiß, N., Bormann, L., Ghosh, D.S., Sonntag, J.M., Jordan, R., Gaponik, N., Leo, K., Eychmüller, A.: Influence of the average molar mass of poly (N-vinylpyrrolidone) on the dimensions and conductivity of silver nanowires. Phys. Chem. Chem. Phys. **21**, 9036–9043 (2019)
29. Zhang, P., Wei, Y., Ou, M., Huang, Z., Lin, S., Tu, Y., Hu, J.: Behind the role of bromide ions in the synthesis of ultrathin silver nanowires. Mater. Lett. **213**, 23–26 (2018)
30. Zhang, Y., Guo, J., Xu, D., Sun, Y., Yan, F.: One-pot synthesis and purification of ultralong silver nanowires for flexible transparent conductive electrodes. ACS Appl. Mater. Interfaces **9**, 25465–25473 (2017)
31. Niu, Z., Cui, F., Kuttner, E., Xie, C., Chen, H., Sun, Y., Dehestani, A., Schierle-Arndt, K., Yang, P.: Synthesis of silver nanowires with reduced diameters using benzoin-derived radicals to make transparent conductors with high transparency and low haze. Nano Lett. **18**, 5329–5334 (2018)
32. Lee, J.H., Lee, P., Lee, D., Lee, S.S., Ko, S.H.: Large-scale synthesis and characterization of very long silver nanowires via successive multistep growth. Cryst. Growth Des. **12**, 5598–5605 (2012)
33. Coskun, S., Aksoy, B., Unalan, H.E.: Polyol synthesis of silver nanowires: an extensive parametric study. Cryst. Growth Des. **11**, 4963–4969 (2011)
34. Prabukumar, C., Bhat, K.U.: Purification of silver nanowires synthesised by polyol method. Mater. Today Proc. **5**, 22487–22493 (2018)
35. Xue, Q., Yao, W., Liu, J., Tian, Q., Liu, L., Li, M., Lu, Q., Peng, R., Wu, W.: Facile synthesis of silver nanowires with different aspect ratios and used as high-performance flexible transparent electrodes. Nanoscale Res. Lett. **12**, 480 (2017)
36. Ćwik, M., Buczyńska, D., Sulowska, K., Roźniecka, E., Mackowski, S., Niedziółka-Jönsson, J.: Optical properties of submillimeter silver nanowires synthesized using the hydrothermal method. Materials **12**, 721 (2019)
37. Wiley, B., Sun, Y., Mayers, B., Xia, Y.: Shape-controlled synthesis of metal nanostructures: the case of silver. Chem. A Eur. J. **11**, 454–463 (2005)
38. Amendola, V., Pilot, R., Frasconi, M., Maragò, O.M., Iatì, M.A.: Surface plasmon resonance in gold nanoparticles: a review. J. Phys. Condens. Matter **29**, 203002 (2017)
39. Larcher, D., Gerand, B., Tarascon, J.M.: Low temperature synthesis of γ-Li_xMnO_2 powders in ethylene glycol. Int. J. Inorg. Mater. **2**, 389–396 (2000)
40. Wang, S., Tian, Y., Ding, S., Huang, Y.: Rapid synthesis of long silver nanowires by controlling concentration of Cu^{2+} ions. Mater. Lett. **172**, 175–178 (2016)
41. Haacke, G.: New figure of merit for transparent conductors. J. Appl. Phys. **47**, 4086–4089 (1976)

42. Sepulveda-Mora, S.B., Cloutier, S.G.: Figures of merit for high-performance transparent electrodes using dip-coated silver nanowire networks. J. Nanomater. (2012). https://doi.org/10.1155/2012/286104
43. Ha, B., Jo, S.: Hybrid Ag nanowire transparent conductive electrodes with randomly oriented and grid-patterned Ag nanowire networks. Sci. Rep. **7**, 11614 (2017)